J Mater Sci (2018) 53:11883–11900

Polymers

Dialdehyde cellulose nanocrystal/gelatin hydrogel optimized for 3D printing applications

Yani Jiang[1], Jiping Zhou[2,*], Zhe Yang[1], Dongfang Liu[2], Xiaodong Xv[1], Guoqi Zhao[1], Hongcan Shi[3], and Qi Zhang[2]

[1] College of Animal Science and Technology, Yangzhou University, No. 48 East Wenhui Road, Yangzhou, Jiangsu, China
[2] College of Mechanical Engineering, Yangzhou University, No. 196 West Huayang Road, Yangzhou, Jiangsu, China
[3] Medical College, Yangzhou University, No. 11 Huaihai Road, Yangzhou, Jiangsu, China

Received: 2 March 2018
Accepted: 3 May 2018
Published online: 14 May 2018

ABSTRACT

Three-dimensional (3D) printing, used to fabricate modular and patient-specific scaffolds with high structural complexity and design flexibility, has drawn wide attentions in the tissue engineering area. However, one of the key problems hindering the application and development of 3D printing in TE area is the poor mechanical property of bio-inks. In this work, we aimed to design a high-strength hydrogel system based on dialdehyde cellulose nanocrystals (DAC) and gelatin (GEL) as a new bio-ink for 3D printing of scaffolds. The DAC were prepared and used as a natural crosslinker to interact with the GEL through a Schiff base reaction. The mechanical test results indicated that the breaking strength of the optimal 4:8-DAC/GEL sample was almost 41.3-fold greater than that of the GEL hydrogel. According to the rheological test results, the 4:8-DAC/GEL sample incubated for 3 h was proposed as a bio-ink for 3D printing. Then, the printing conditions, including the printing pressure and nozzle speed, as well as additional crosslinking conditions for a freshly printed scaffold, i.e., the crosslinking time and temperature, were optimized. Crosslinked scaffolds with adjustable porosity and good fidelity were successfully obtained. The biocompatibility of 4:8-DAC/GEL was also investigated by CCK-8 and Hoechst 33342/PI double-staining assays. Collectively, these results confirm the good potential of the 4:8-DAC/GEL hydrogel as a 3D bio-ink for application in tissue repair.

Introduction

Tissue engineering has (TE) played a significant role in the medical field, with an ever-growing demand for various tissue donations since its inception [1]. However, without a three-dimensional (3D) complex geometry, the artificial tissue scaffold can not transport nutrients or exchange and remove wastes in the human body. With the development of three-dimensional (3D) printing technologies, fabrication of complex tissue scaffolds may come true [2].

Address correspondence to E-mail: jpzhou@yzu.edu.cn

https://doi.org/10.1007/s10853-018-2407-0

Hydrogels, with 3D network structures and water contents of approximately 90% and similarities to the human soft tissues [3], such as skin, cartilage, tendons, ligaments and muscles, have attracted considerable attention as biomaterials for preparation of implantable scaffold in the TE field [4]. To date, hydrogels based on natural biopolymers, such as alginate [5, 6], gelatin (GEL) [7, 8], collagen (COL) [9], COL and fibrin [10], hyaluronic acid [11], chitosan and agarose [1, 12], have been demonstrated to fulfill essential requirements for cell cultures and used to prepare scaffolds through 3D printing. However, mainly of these natural hydrogels present poor mechanical properties. For instance, GEL, which is extracted from animal sources, exhibits many excellent properties, such as good biocompatibility, bioactivity, and biodegradability, along with low antigenicity and the promotion of such processes as cell proliferation, differentiation, and platelet aggregation; however, their applications for 3D printing were still limited due to their low mechanical strength [13].

Many methods have been adopted to improve the mechanical strength for these hydrogel bio-inks. Tan et al. [14] created a novel bio-ink which constituted of poly (D-,L-lactic-co-glycolic acid) (PLGA) porous microspheres with a thin encapsulation of agarose-COL composite hydrogel (AC hydrogel), which proved to have a compressive strength more than 100 times that of pure AC hydrogel. Li et al. [3] added graphene oxide into alginate for improving both mechanical strength and rheological property of the bio-ink. Kim et al. [15] printed cell-blocks using COL as bio-ink followed by crosslinking treatment with genipin to improve mechanical properties of the printed construct. In summary, methods for improving the mechanical properties of bio-inks can be divided into three categories: (1) Improving the interfacial interaction and crack resistance by introduction of a reinforcer [3, 16]; (2) Blending modification by introducing other hydrogels [17, 18]; (3) Forming a crosslinking structure by adding a crosslinker [15].

Nanocellulosic materials isolated from plant cellulose are also attractive as TE materials due to their high aspect ratio, high strength, abundant hydroxyl groups and good biocompatibility [19]. It is not surprising that cellulose nanocrystals (CNC) and nanofibers (CNF) have been applied for 3D printing. The CNC (or CNF) can be used as a reinforcer or blending modifier to improve the mechanical strength of hydrogel bio-inks, such polyvinyl alcohols [20], hyaluronic acid [18, 21], alginate [21–24], or as a viscosity modifier to improve the viscosity of bio-ink [25]. In addition, the single CNC or CNF suspension as a direct bio-ink also has been attempted [26, 27]. Dialdehyde cellulose nanocrystals (DAC), a derivative of CNC, have been reported as a natural crosslinker for the GEL or COL through Schiff's base reaction in the field of traditional biomedical materials [4, 28]. This natural crosslinker can avoid formation of toxic residue from chemical crosslinking agents like glutaraldehyde, formaldehyde, and carbodiimide [4, 28]. Base on these advantages, we used DAC as an crosslinked agent to improve the mechanical strength of the GEL bio-ink. It is also important to know whether this DAC/GEL hydrogel, as a new bio-ink, is suitable for 3D printing.

In this paper, we aimed to design a high-strength DAC/GEL-based hydrogel and investigate its potential as a bio-ink for 3D printing applications. The CNC were isolated from *Humulus japonicus* stems (HJS) and later oxidized into DAC to prepare the DAC/GEL hydrogel. The aldehyde content of the DAC was determined using the sodium hydroxide titration method. The structural characteristics of the CNC, DAC, GEL, and DAC/GEL were investigated by Fourier transform infrared spectroscopy (FTIR). Then, the swelling behavior and mechanical properties of DAC/GEL hydrogels with different mass ratios (1:8, 2:8, 3:8, 4:8) were investigated to choose a suitable hydrogel. Next, the rheological properties of the 4:8-DAC/GEL hydrogel were further investigated for 3D printing. Subsequently, the printability of the proposed 4:8-DAC/GEL hydrogel incubated for 3 h was investigated with the aim to generate 3D printed scaffolds with tunable porosity and good fidelity through optimization of the printing pressure and nozzle speed. Finally, the biocompatibility of 4:8-DAC/GEL was also investigated by Cell Counting Kit 8 (CCK-8) and Hoechst 33,342/propidium iodide (PI) double-staining assays.

Materials and methods

Materials

Gelatin was of biological reagent grade and purchased from the Macklin Biochemical Reagent Co., Ltd. (Shanghai, China). Other chemicals were of analytical reagent grade.

Methods

Preparation of CNC

CNC were prepared by the sulfuric acid hydrolysis method. The details of this method were reported in our previous study [29]. Briefly, the HJS powder was treated with 4% sodium hydroxide solution (W_{HJS}/V_{NaOH} = 1/15) at 80 °C for 2 h and treated 3 times with 5% acidified sodium chlorite (W_{HJS}/V_{ASC} = 1/15) at 80 °C for 6 h (2 h each time) to remove hemicellulose and lignin. Next, the bleached HJS powder was hydrolyzed using 60% sulfuric acid (W_{HJS}/V_{acid} = 1/20) at 45 °C for 1 h with strong agitation. The reaction was terminated by the addition of a volume of water 10 times that of the reaction solution. The suspension was filtered and subsequently centrifuged and dialyzed (8000–10000D, RC) until its pH became constant. This process is known to produce finely divided CNC.

Preparation of DAC

DAC were prepared using a method reported by Lu et al., with some modifications [28]. Briefly, CNC were oxidized into DAC by sodium periodate with amass ratio of 1:2 ($W_{CNC}/W_{Sodium\ periodate}$) at a temperature of 40 °C for different periods and were preserved away from light. Then, the reaction products were washed with triple-distilled water to remove the reduction product of sodium iodide and the unreacted sodium periodate. The suspension was filtered, centrifuged and dialyzed (8000–10000D, RC) until its total dissolved solids (TDS) (measured using TDS meter) value reached zero. The DAC with an aldehyde content of 49.39% were used in the following experiment (details can be seen in supplements).

Preparation of DAC/GEL composite hydrogel

An amount of GEL was added into phosphate-buffered solution (PBS) and stirred at 40 °C until it was completely dissolved to produce an 8% GEL solution. Different concentrations of DAC suspensions (1, 2, 3, 4%) were separately added to the 8% GEL solution at a volume ratio of 1:1. In addition, a 4% CNC suspension was blended with the 8% GEL solution at a volume ratio of 1:1. The diluted GEL with a concentration of 4% was used as a control sample. If not otherwise specified, these samples were all stirred at 37 °C for 1 h and then incubated at 37 °C for 24 h followed by 4 °C for 4 h to form hydrogels. These hydrogel samples are referred to as 1:8-DAC/GEL, 2:8-DAC/GEL, 3:8-DAC/GEL, 4:8-DAC/GEL, 4:8-CNC/GEL and GEL. These samples and their compositions are listed in Table 1.

Characterization

FTIR

All sample solutions were poured into Teflon molds, and their films were stripped off after drying. The FTIR spectra of the samples were characterized with a Fourier transform infrared spectrometer (670-IR +610-IR Varian, Varian Co., Ltd., USA). Their spectra were recorded at a resolution of 4 cm^{-1} from 400 to 4000 cm^{-1}.

X-ray photoelectron spectroscopy (XPS)

The surface elements and chemical state of the samples were analyzed using a K-Alpha X-ray photoelectron spectrometer (Thermo Fisher Scientific, USA). The samples were excited by a monochromatic Al Kαray and radiated by an X-ray beam at 6 mA, with a sensitivity of 350 kcps and energy resolution of 0.5 eV.

Swelling behavior in PBS (phosphate buffer solution)

In this experiment, the swelling properties of 1:8-DAC/GEL, 2:8-DAC/GEL, 3:8-DAC/GEL and 4:8-DAC/GEL were investigated. The hydrogel samples were immersed in PBS (pH = 7.4) at 37 °C until swelling equilibrium was reached. The swelling ratios (SR) of the hydrogel samples were calculated as follows:

Table 1 Chemical composition of hydrogel samples

Samples	Mass ratio of DAC (CNC)/GEL $M_{DAC(CNC)}$:M_{GEL}	Content of GEL C_{GEL}(mg mL^{-1})	Content of DAC or CNC $C_{DAC\ (CNC)}$ (mg mL^{-1})	Content of total solids C_{Total} (mg mL^{-1})
GEL	–	40	0	40
1:8-DAC/GEL	1:8	40	5	45
2:8-DAC/GEL	2:8	40	10	50
3:8-DAC/GEL	3:8	40	15	55
4:8-DAC/GEL	4:8	40	20	60
4:8-CNC/GEL	4:8	40	20	60

$$SR = \frac{V_t}{V_0} \quad (1)$$

where V_t is the volume of swollen hydrogel at adsorption time t, and V_0 is the volume of the hydrogel sample before absorbing water. The results are the averages of five samples.

Mechanical property measurements

The mechanical properties of the hydrogel samples were measured via a uniaxial compression test method using a universal tensile testing machine (HLD-0824, Handpi Co., Ltd., China). The hydrogel samples were cylindrical with a diameter of 15 ± 1 mm and a height of 10 ± 1 mm. The tests were performed at a compression speed of 0.5 mm s^{-1} at 15 °C. The results are the averages of at least five samples.

Rheological characterization

A discovery hybrid rheometer (DHR-3, TA instruments Co., Ltd., USA) was used to evaluate the rheological properties of the hydrogel samples.

First, the strain amplitudes of the hydrogel samples (4:8-DAC/GEL, 4:8-CNC/GEL and GEL) were verified to ensure that the measurements were conducted within the linear viscoelastic region (LVR). The hydrogel samples were analyzed at a temperature rate of 3 °C min^{-1} from 3 to 50 °C in oscillation mode using a strain of 1% and a frequency of 1 Hz.

Second, the storage modulus (G'), loss modulus (G''), and viscosity were separately monitored as a function of time for 8 h at 1 Hz and 1% strain under a constant temperature of 37 °C.

Third, the viscosity of the 4:8-DAC/GEL hydrogel was measured at shear rates ranging from 0.1 to 100 s^{-1} at room temperature.

3D printing

The 4:8-DAC/GEL hydrogel incubated for 3 h was printed using a 3D bioprinter (Bio-Architect, Life/Pro, Regenovo Biotechnology Co., Ltd., China). Scaffolds were designed and input into the printer software. The printing process was conducted using an extrusion-based printing nozzle with diameter of 210 μm, and the hydrogel flow was controlled by a pressure regulator.

First, the printability of the 4:8-DAC/GEL hydrogel incubated for 3 h was evaluated by printing a single filament with length of 30 mm using a combination of different printing pressures (0.1–0.25 MPa) and nozzle moving speeds (10–40 mm s^{-1}). Second, scaffolds with different shapes were printed in a layer-by-layer manner to verify the optimal printing conditions. A total of four layers were printed for every construct with a filament spacing of 710 μm (theoretical pore

diameter = 500 μm). The macromorphology of the filaments and the printed scaffolds were observed using a digital camera (S2900HD, FinePix Co., Ltd., Japan). The filament width was measured using a digital image-processing program (Image J, National Institutes of Health, USA). The results are the averages of five samples.

Crosslinking efficiency of the printed scaffold

The ε-amino groups of lysine in GEL or unreacted GEL in the printed 4:8-DAC/GEL scaffold can react with 2,4,6-trinitrobenzene sulfonic acid (TNBS) to form a soluble complex. The crosslinking efficiency was determined by comparing the lysine content of pure GEL and the printed 4:8-DAC/GEL scaffold using a TNBS assay, as proposed by Bunins [30].

In this experiment, the 4:8-DAC/GEL scaffolds were sealed in glass containers and kept at different temperatures for different periods. Then, these scaffold samples were separately mixed with tri-distilled water followed by strong agitation to form uniformly diluted suspensions with the same GEL content of 1 mg mL^{-1} and DAC content of 0.5 mg mL^{-1}. Subsequently, 1 mL of 4% (w/v) sodium bicarbonate solution and 1 mL of freshly prepared 0.1% TNBS solution were added to 1 mL of the GEL solution (C_{gel} = 1 mg mL^{-1}) and 1 mL of the DAC suspension (C_{DAC} = 0.5 mg mL^{-1}), and the diluted suspension was stirred at 40 °C for 4 h. This mixed solution was treated with 6 M HCl at a ratio of 1:3 (v/v) at 40 °C for 1.5 h; then, the absorbance at 334 nm was measured after dilution.

The crosslinking efficiency was calculated as follows:

$$\text{Crosslinking efficiency (\%)} = \frac{A_{GEL} - A_{DAC} - A_{4:8-DAC/GELscaffold}}{A_{GEL}} \times 100\% \quad (2)$$

where A_{GEL}, A_{DAC} and $A_{4:8\text{-}DAC/GEL\ scaffold}$ are the absorbances of the diluted GEL solution, the diluted DAC solution and the unreacted GEL in the printed 4:8-DAC/GEL scaffold. The results are the averages of three samples.

Physical characteristics of the crosslinked scaffold

Macromorphology of the crosslinked scaffold (crosslinked for 21 h at 37 °C) was captured using a digital camera (S2900HD, FinePix Co., Ltd., Japan). The micromorphology of the crosslinked scaffold after lyophilization was characterized by scanning electron microscopy (SEM, S-4800, Hitachi Co., Ltd., Japan) after being sputtered with gold. The images were captured at an accelerating voltage of 15 kV. The pore diameter was measured using a digital image-processing program (Image J, National Institutes of Health, USA). The results are averages of 50 representative pores.

The porosity of the crosslinked scaffold after lyophilization was calculated according to the liquid substitution method [31]. First, the length (l), width (w) and height (h) of the scaffold were measured. The total volume of the printed scaffold was calculated as l × w × h. Ethanol was used in this experiment because it could easily penetrate the pores of the scaffold and did not induce shrinkage or swelling of the material. The printed scaffold was immersed in a graduated cylinder containing an amount of ethanol (V_1) for 5 min. Then, the total volume of the ethanol and the scaffold was recorded as V_2. The volume difference ($V_2 - V_1$) represents the volume of the scaffold. The results are the averages of five samples

$$\text{Porosity (\%)} = \frac{l \times w \times h - (V_2 - V_1)}{l \times w \times h} \times 100\% \quad (3)$$

Water absorption was assessed using a previously described method [32]. The crosslinked scaffold after lyophilization was precisely weighed and then immersed in distilled water for 20 min. After immersion, the scaffold was left to stand in a culture dish for 1 min; then, the weight was measured again. The water absorption was calculated as follows:

$$\text{Water absorption (\%)} = \frac{W_t - W_0}{W_0} \times 100\% \quad (4)$$

where W_t denotes the weight of the scaffold after absorbing water, and W_0 denotes the weight of the scaffold before absorbing water. The results are the averages of five samples.

Shrinkage was a deformation extent of the crosslinked scaffold compared to the freshly printed scaffold. The shrinkage rate was calculated as follows:

$$\text{Shrinkage rate (\%)} = \frac{L_C - L_F}{L_F} \times 100\% \quad (5)$$

where L_C and L_F stand for the size of the crosslinked scaffold and freshly printed scaffold, respectively. The results are the averages of five scaffolds.

In vitro cytotoxicity and cell morphology

The 4:8-DAC/GEL hydrogel was immersed in Dulbecco's Modified Eagle's Medium (DMEM) with fetal bovine serum (FBS, 10%) and pen/strep (1%) and left overnight, followed by centrifugation to collect the leaching liquor.

Cell growth inhibition was studied by CCK-8 assay (Dojindo, Shanghai, China) according to the manufacturer's instructions. The leaching liquor was used as the 3T3 cell growth medium. In total, 1.0×10^3 3T3 cells per well were seeded in 96-well plates with 100 μL of leaching liquor and incubated (37 °C, 5% CO_2) for 1, 3, 5, and 7 days. Five independent samples were used for each time interval and experimental group. Then, 10 μL of the CCK-8 reagent was added to each well, and the cells were continuously incubated for 2 h. To determine the number of proliferating cells, the absorbance at 450 nm was measured for each well using an auto-microplate reader (Thermo Scientific, Shanghai, China).

To examine whether the hydrogel induced apoptosis, a Hoechst 33,342/PI double-staining assay was carried out. 3T3 cells were cultured in 24-well plates with the leaching liquor for 48 h. At the 48-h point, cell morphology was assessed using an Apoptosis and Necrosis Assay Kit (Beyotime Institute of Biotechnology, Shanghai, China). Briefly, cells in the 24-well plates were washed twice with PBS (pH = 7.4) and then stained with Hoechst 33,342 (10 ng mL^{-1}) and PI (10 ng mL^{-1}) for 20 min at 4 °C in the dark. The condensed or fragmented nuclei of apoptotic cells were observed by fluorescence microscopy.

To observe the morphological differences of the cells, the 3T3 cells were seeded on a hydrogel coating with a thickness of 2 mm and cultured with DMEM, FBS (10%) and pen/strep (1%) for 7 days. After the medium was discarded, the hydrogel coating was washed three times with PBS. Then, the hydrogel coating was fixed with 2.5% glutaraldehyde, washed with PBS, dehydrated with an ethanol gradient (50, 70, 80, 90, 100%) and dried with a critical-point dryer. Finally, the morphology of the 3T3 cells was observed using a field emission scanning electron microscope (FE-SEM, S-4800, Hitachi Co., Ltd., Japan) after sputtering the samples with gold.

Statistical analysis

Data are expressed as the means of at least three replicates ± standard deviation (SD). The results were analyzed by analysis of variance (ANOVA). LSD multiple comparison tests were used to determine significant differences between the mean values. Significant differences between two groups were determined using two-tailed Student's t tests. A confidence level of 95% ($P < 0.05$) was used, and the analyses were performed using SPSS software version 17.0 (SPSS, Inc., Chicago, USA).

Results and discussion

Analysis of chemical crosslinkings between DAC and GEL

The FTIR spectra of the CNC, DAC, GEL and DAC/GEL samples are shown in Fig. 1a. The prominent absorption peaks at 3402 and 2900 cm^{-1}, which were observed for both CNC and DAC, represent the stretching vibrations of O–H and C–H in cellulose [33, 34]. Two characteristic absorption peaks were observed in the DAC spectrum: one at approximately 1730 cm^{-1}, which was attributed to the characteristic absorption peak of the aldehyde group (C=O); and the other at 892 cm^{-1}, corresponding to the bending vibration of –CH of the aldehyde group [35]. These results indicated that a successful oxidization reaction occurred on the molecular chain of the CNC, with the production of aldehyde groups. The GEL was characterized by its peaks at 1628 cm^{-1} due to the C=O stretching vibration of amino I [36], at 1539 cm^{-1} due to the N–H bending vibration of amino II, and at 1238 cm^{-1} due to the N–H deformation of amino III [36]. Nevertheless, the peak at 1660 cm^{-1} for C=N (Schiff's base) was not observed in our measurements, because the stronger amide I bands might mask the band [28]. Therefore, XPS was performed to further determine the surface elements and chemical state of the samples.

According to a report by Dorris et al., the element carbon in wood is divided into four bonding forms, namely, C1, C2, C3 and C4:C1, unoxidized carbon (C–C); C2, carbon with one oxygen bond (C–O); C3, carbon with two oxygen bonds (O–C–O or C=O); and C4, carbon with three oxygen bonds (O–C=O) [37]. These four categories reveal C1 s peaks at 285.0,

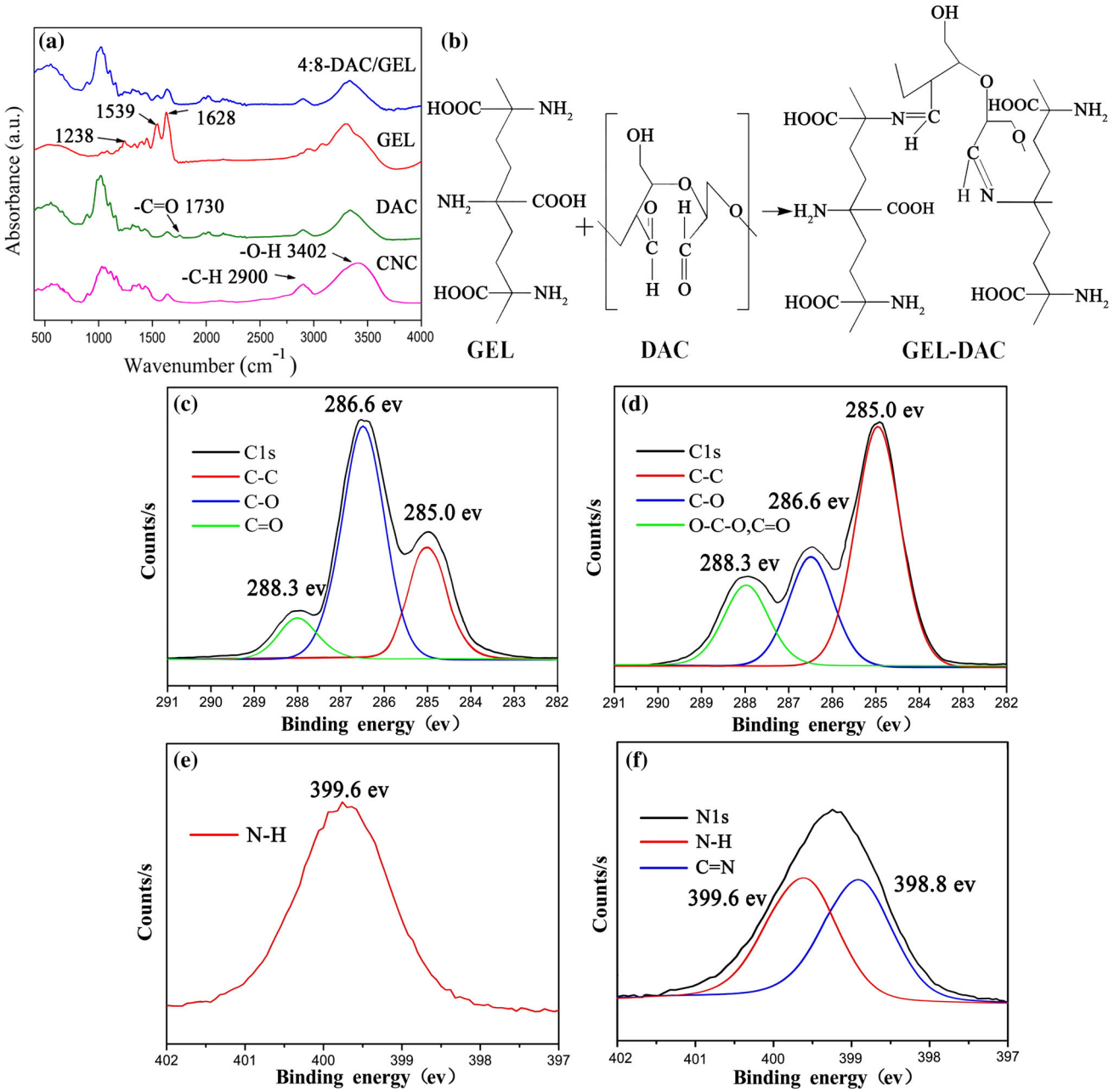

Figure 1 FTIR spectra (**a**) of the CNC, DAC, GEL, 4:8-DAC/GEL samples. A sketch of crosslinking reaction between a DAC and GEL (**b**). C1 s high-resolution XPS spectra of CNC (**c**) and DAC (**d**). N1 s high-resolution spectra XPS of GEL (**e**) and 4:8-DAC/GEL (**f**).

286.6, 288.3 and 289.5 eV, respectively. In the high-resolution spectra of the CNC (Fig. 1c) and the DAC (Fig. 1d) samples, the C3 content was significantly greater in the DAC than the CNC, indicating that the C2 carbons transformed to C3 carbons after periodate oxidation. In addition, the high-resolution spectra of N1 s for GEL and 4:8-DAC/GEL are displayed in Fig. 1e and f. Note that the –C=N– peak at 398.8 V and N–H peak at 399.6 eV were present in the 4:8-DAC/GEL spectrum, while only the N–H peak at 399.6 eV was observed in the GEL spectrum [38]. This difference indicated that the GEL reacted with the DAC via a Schiff base reaction, as shown in Fig. 1b. The DAC as crosslinker can be further used to react with other natural biopolymers which contain amino groups, such as COL and chitosan.

Swelling ratio

Ideally, minimal swelling behavior is often desired for hydrogels to guarantee their stability at the implantation site and to keep their initial shape of printed scaffolds [39]. Therefore, it is important to evaluate the swelling properties of the hydrogel samples. 1:8-DAC/GEL, 2:8-DAC/GEL, 3:8-DAC/GEL and 4:8-DAC/GEL hydrogel samples were immersed in PBS at 37 °C. Figure 2a shows that the swelling ratios for all the samples varied slowly in the first 3 h. The swelling ratios for 1:8-DAC/GEL, 2:8-DAC/GEL, 3:8-DAC/GEL and 4:8-DAC/GEL were 1.22, 1.15, 1.11 and 1.05 at the 3-h point, respectively. Figure 2b shows that, in the DAC/GEL hydrogel system, hydrogel sample with higher mass ratio of DAC/GEL could maintain its shape for longer time and had lower swelling ratio. As time went on, the differences of swelling ratios among all of the samples became increasingly obvious. The swelling ratios for 1:8-DAC/GEL, 2:8-DAC/GEL, 3:8-DAC/GEL and 4:8-DAC/GEL were 1.93 at the 28-h, 1.73 at the 36-h, 1.54 at the 52-h and 1.37 at the 60-h points, respectively. This result was because that higher DAC/GEL ratio led to a higher crosslinking degree resulting in a denser network structure in the hydrogel. Consequently, there were fewer available free hydrodynamic groups for the accommodation of water molecules in the DAC/GEL hydrogels because of their denser crosslinking network structure (as shown in Fig. 1b), which contributed to a decrease in matrix swelling. In addition, the crosslinking network structure hindered the mobility and relaxation of the polymer chains and simultaneously impeded the diffusion of water molecules, which reduced the swelling ratio.

Mechanical property measurements

Good mechanical properties are required for the successful application of a printed scaffold [32]. Therefore, we aimed to optimize the mechanical strength of the hydrogel by adjusting the DAC/GEL mass ratio in this experiment.

The breaking strengths of the GEL and DAC/GEL hydrogel samples with different mass ratios (1:8, 2:8, 3:8, 4:8) are displayed in Fig. 3a. The breaking strengths of all the DAC/GEL hydrogel samples were significantly improved compared with the pure GEL hydrogel, and the breaking strength increased with increasing DAC/GEL mass ratio. We also added unmodified CNC to the GEL to make the total solid content consistent and then repeated the breaking strength test. The strain–stress curves of the GEL, 4:8-CNC/GEL and 4:8-DAC/GEL samples are shown in Fig. 3b. The breaking strength for the 4:8-CNC/GEL hydrogel was 0.091 MPa, which was approximately 2.22-fold greater than that of the GEL (0.041 MPa), but the breaking strength of the 4:8-DAC/GEL hydrogel was 1.695 MPa, which was almost 41.3-fold greater than that of the pure GEL hydrogel.

Markstedt et al. [22] used CNF as a blending modifier to improve the strength of alginate bio-ink. Due to lack of an effective interaction between the CNF and alginate, the maximal compressive stiffness of the composite bio-ink only reached about 250 kPa. Moreover, Zhang et al. [2] reported the production of strong COL hydrogels by crosslinking modification

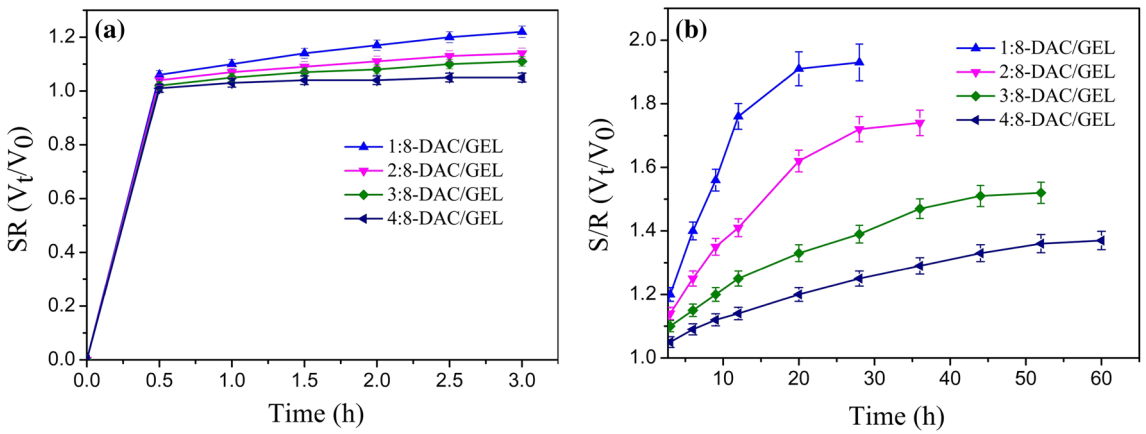

Figure 2 Change of swelling ratio (SR) of the 1:8-DAC/GEL, 2:8-DAC/GEL, 3:8-DAC/GEL and 4:8-DAC/GEL with increasing time, $P < 0.05$.

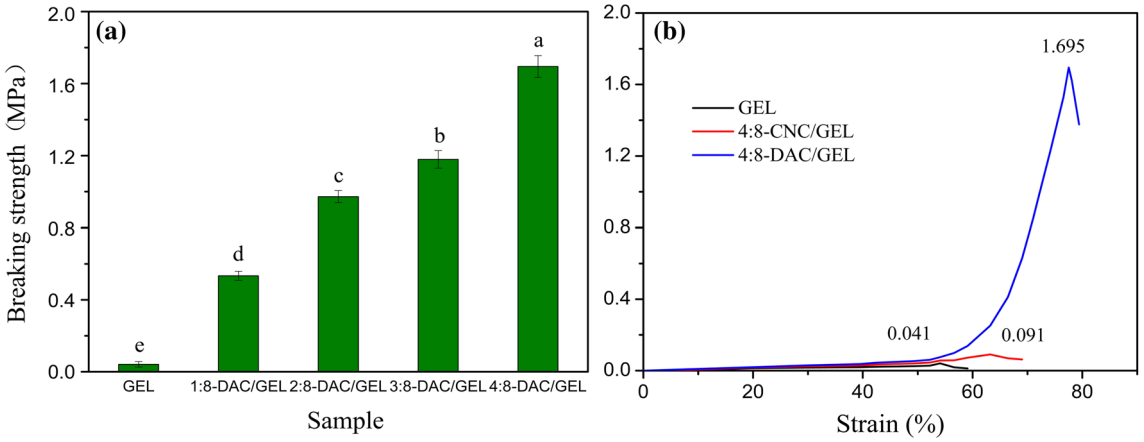

Figure 3 Breaking strengths (**a**) of GEL, 1:8-DAC/GEL, 2:8-DAC/GEL, 3:8-DAC/GEL and 4:8-DAC/GEL. Strain–stress curves (**b**) of GEL, 4:8-CNC/GEL and 4:8-DAC/GEL. Different letters indicate a significant difference between samples ($P < 0.05$).

with aldehyde-functionalized dextran (DAD). The maximum compressive strength of the COL/DAD hydrogel was approximately 40.6-fold greater than that of the pristine COL hydrogel. In our work, the compression breaking strength of 4:8-DAC/GEL was 41-fold greater than that of the pure GEL. This result further supported our assumption that the DAC serves as a macromolecular crosslinker for the GEL, forming a network and resulting in a significant increase in the strength of the DAC/GEL hydrogel. In addition, this modification method could be applied to improve the mechanical strength of other GEL-equivalent bio-inks such as COL and chitosan, which could also crosslink with DAC.

Based on the results of mechanical property measurements and swelling behavior, the 4:8-DAC/GEL which had the highest mechanical strength and lowest swelling ratio was proposed for further investigation for 3D printing.

Rheological properties

In this section, the theological properties of 4:8-DAC/GEL were investigated. The conditions for the hydrogel samples and the test conditions for each experiment are listed in Table 2.

$T_{sol–gel}$ is defined as the temperature at which the storage modulus (G') intersects the loss modulus (G''). This parameter indicates that the material can appear to be in a sol state or gel state if the ambient temperature is higher or lower than $T_{sol–gel}$, respectively. GEL is a well-known thermosensitive polymer; therefore, it was necessary to investigate the $T_{sol–gel}$ of the hydrogel samples by evaluating rheological properties at varying temperatures. The storage and loss moduli of the hydrogel samples were studied at temperatures ranging from 3 to 50 °C within the LVR. Figure 4a shows that the $T_{sol–gel}$ of the GEL and 4:8-CNC/GEL samples was 23.8 and 30.7 °C, respectively. However, the G' and G'' of the 4:8-DAC/GEL sample changed slowly with increasing temperature, and there was no intersection of G' and G'' for 4:8-DAC/GEL in the temperature range from 3 to 50 °C. As such, the GEL and 4:8-CNC/GEL hydrogels would be not suitable for the direct construction of tissue-engineered scaffolds because the GEL and the 4:8-CNC/GEL hydrogel samples with low $T_{sol–gel}$ values (23.8, 30.7 °C) would transit into the sol phase after transplantation into the human body (approximate to 37 °C) and be unable to provide stress support for tissue repair.

To characterize the effect of the incubation time on the formation of the 4:8-DAC/GEL hydrogel, we performed further rheological testing. The 4% DAC suspension was added to the 8% GEL solution at a volume ratio of 1:1 and quickly stirred evenly. Then, the rheology test was performed at 37 °C. Figure 4b shows that the G' of the 4:8-DAC/GEL hydrogel started to increase significantly after approximately 1 h of incubation from 90.12 Pa at 1 h to 349.96 Pa at 2 h and to 5297.23 Pa at 4 h. This result indicated that the network structure of the hydrogel was constantly forming and improving during this period. The increase in G' indicated an improvement in the rigidity of the hydrogel, which was due to the formation of the 3D network structure and the increasing degree of integration between macromolecules in

Table 2 Pretreatment and test conditions of hydrogel samples for all rheological tests

Samples	Pretreatment conditions			Test conditions		
	Period of stirring	Period of incubation	Period of storing at 4 °C	Test program	Temperature of test	Period of test
GEL	1 h	24 h	4 h	$G'(G')$-temperature (Fig. 5a)	3–50 °C	–
4:8-CNC/GEL	1 h	24 h	4 h			
4:8-DAC/GEL	1 h	24 h	4 h			
4:8-DAC/GEL	Quickly stirred evenly	_	_	$G'(G')$-time (Fig. 5b)	37 °C	0–8 h
4:8-DAC/GEL	Quickly stirred evenly	_	_	Viscosity–time (Fig. 5c)	37 °C	0–8 h
4:8-DAC/GEL	Quickly stirred evenly	3 h	_	Viscosity–rate (Fig. 5c)	37 °C	0–8 h

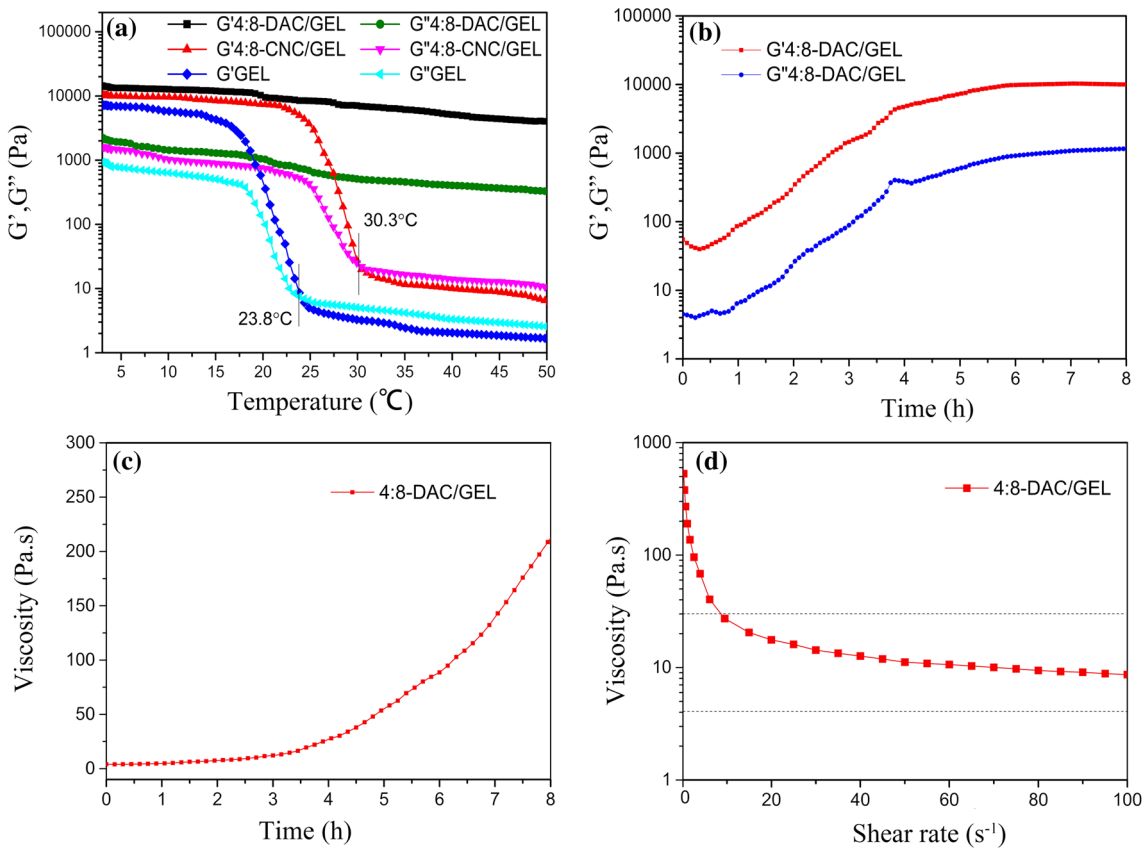

Figure 4 Change in storage modulus (G') and loss modulus (G') of the GEL, 4:8-CNC/GEL and 4:8-DAC/GEL hydrogels with increasing temperature (**a**). Change in storage modulus (G') and loss modulus (G') of the 4:8-DACl/GEL hydrogel with increasing incubation time (**b**). Change in viscosity of the 4:8-DACl/GEL hydrogel with increasing incubation time (**c**). Change in viscosity of the 4:8-DAC/GEL hydrogel with increasing shear rate (**d**).

the 4:8-DAC/GEL hydrogel. A higher G' is beneficial for hydrogels to maintain better shape fidelity in the 3D printing process.

As excessively high viscosity could impede hydrogel extrusion through the print head in the 3D printing process, it was important to investigate the variation in the viscosity of 4:8-DAC/GEL. Similarly, the 4% DAC suspension was added to the 8% GEL solution at a volume ratio of 1:1 and quickly stirred evenly. Next, the rheology test was performed at 37 °C. As is well established, to achieve migration of the center of gravity, larger molecules require more incidences of chain coordination. Crosslinking between the DAC and GEL caused an increase in molecular weight. Therefore, the shear viscosity of the polymer increased with the incubation time, as shown in Fig. 4c. The viscosity of 4:8-DAC/GEL at 1, 2, 3 and 4 h was 5.71, 14.06, 29.11 and 152.98 Pa s, respectively. It has been reported that the suitable viscosity of bio-ink ranges from 4 to 30 Pa s for extrusion-based printing [40]. The longer incubation time resulted in a higher G' of the hydrogel, which could offer better shape fidelity but also cause increased viscosity, potentially hindering hydrogel extrusion through the print head in the 3D printing process. Therefore, the incubation time of 3 h was considered a suitable choice for using 4:8-DAC/GEL as bio-ink.

In the process of 3D printing, extrusion pressure could generate a shear rate of approximately 20–60 s^{-1} according to Yeong et al. [41]. Therefore, it was necessary for us to investigate how the varying shear rates affect the viscosity of 4:8-DAC/GEL after incubation for 3 h, and hence its suitability as bio-ink. Ideally, the viscosity of a printable hydrogel should decrease to facilitate flow through the needle [3, 41]. Figure 4d shows that the viscosity of the hydrogel samples decreased with increasing shear rate, revealing that the samples exhibited clear shear-thinning (i.e., pseudo-plastic) behavior. This phenomenon can be attributed to the temporary destruction of the physical interactions and alignment of the polymer chains caused by a high shear rate. Furthermore, it was observed that when the shear rate increased from 20 to 60 s^{-1}, the viscosity decreased from 17.60 to 10.62 Pa s, which was within the proposed range (4–30 Pa s). Supported by the viscosity–time test results, the 4:8-DAC/GEL incubated for 3 h was proposed as bio-ink for 3D printing.

Optimizing 3D printing

Currently, there are two primary printing methods: one is to print the hydrogel and cells separately; the other is to deposit cell-laden hydrogel. The former model can offer better control over the cell distribution in each printed layer [42]. As such, we focused on the extrusion-based printing of acellular biomaterials. The 4:8-DAC/GEL hydrogel incubated for 3 h was used as bio-ink in this printing process.

According to the principle of rapid prototyping, the ratio of the feed rate to the nozzle speed is the main factor affecting the filament width, which affects the precision of printing the scaffolds [42]. Therefore, it was necessary to optimize the 3D printing process by adjusting the 3D printing pressure and the nozzle speed. Images of hydrogel filaments printed using a combination of different pressures and nozzle speeds are shown in Fig. 5a–d. Variations in filament widths are presented in Fig. 5e. Keeping the nozzle speed constant, the filament width increased with increasing printing pressure. When we kept the nozzle speed at 10 mm s^{-1} and increased the printing pressure to 0.25 MPa (Fig. 5a), the filament width reached a maximum of 700 μm. This result occurred because when the nozzle speed is small but the relative extrusion rate of the hydrogel is too large, the extruded hydrogel cannot fully stretch, resulting in excessive accumulation of the hydrogel on the work stage. Such excessive accumulation could reduce the mesh size or cause a lack of pores in the printed scaffold. In addition, as shown in Fig. 5a-e, keeping the printing pressure constant, the filament width decreased with increasing nozzle speed. When we kept the printing pressure at 0.1 MPa and increased the nozzle speed to 40 mm s^{-1} (Fig. 5c, d), the filament width reached a minimum of 220 μm. This occurred because that the amount of extruded hydrogel was small but the nozzle speed was relatively fast, resulting in over stretching of the filaments on the work stage. This overstretching could cause filament breakage and collapse of the printed scaffold. Based on these results, the printing pressure of 0.15 MPa and nozzle speed of 30 mm s^{-1} were used in the 3D printing process because the filaments produced under these conditions exhibited a small width and smooth appearance (Fig. 5c).

Next, scaffolds were printed in different shapes to investigate the optimal combination of printing

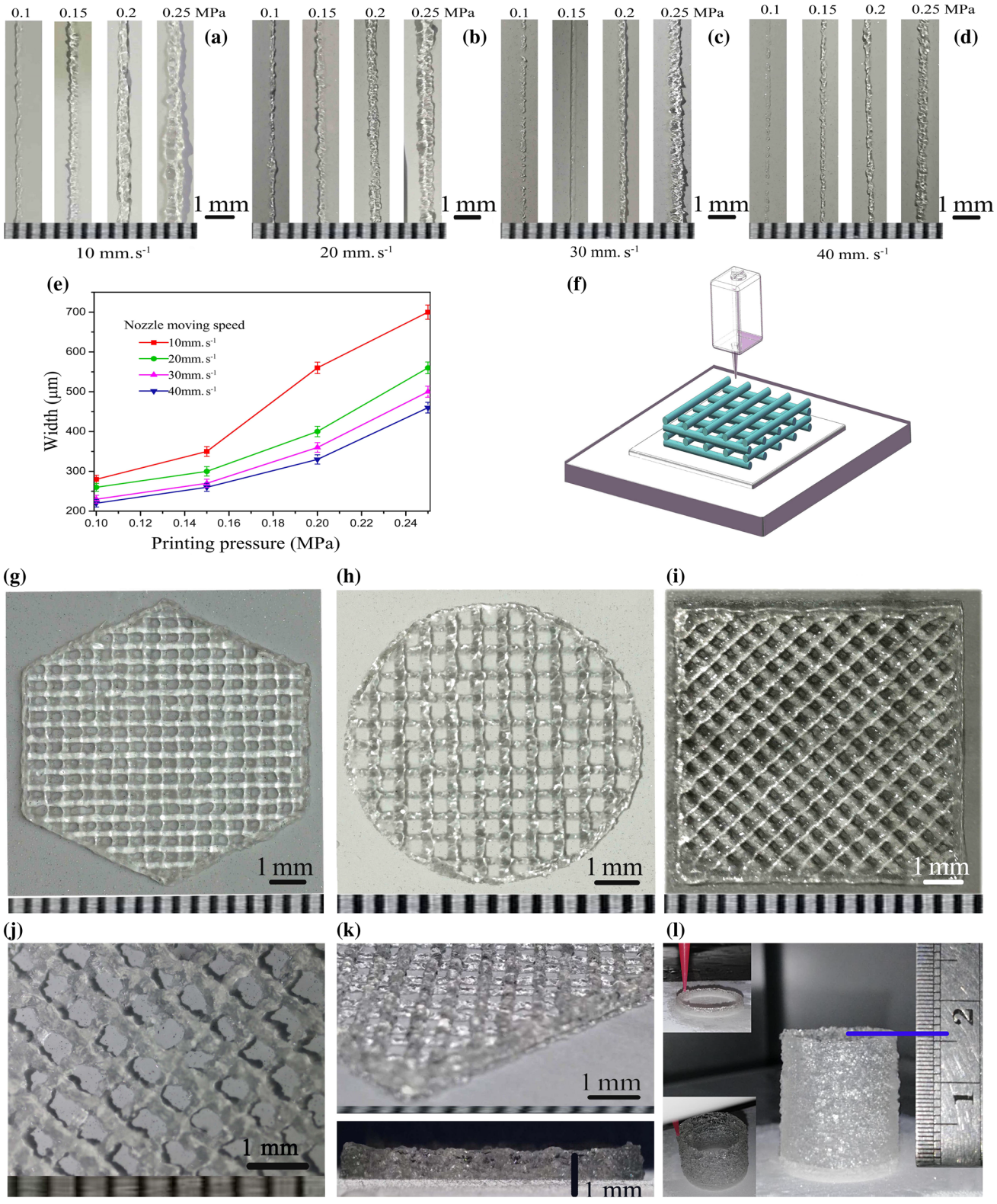
0.1
0.15
0.2
0.25 MPa
(a)
(b)
(c)
(d)
1 mm
10 mm.s-1
20 mm. s-1
30 mm. s-1
40 mm. s-1
(e)
Nozzle moving speed
10mm. s-1
20mm. s-1
30mm. s-1
40mm. s-1
Width (μm)
Printing pressure (MPa)
(f)
(g)
(h)
(i)
(j)
(k)
(l)

◀**Figure 5** Images of filaments (**a**, **b**, **c**, **d**) printed using a combination of different printing pressures (0.1, 0.15, 0.2, 0.25 MPa) and nozzle speeds (10, 20, 30, 40 mm s^{-1}). Effect of printing pressure and nozzle speed on printed filament width (e, $P < 0.05$). Scheme of 3D scaffold printing technique (**f**). Images of 4:8-DAC/GEL scaffold fabricated in a regular hexagon (**g**), circle (**h**), square (**i**). Magnified photograph of some part of scaffold (**j**), Oblique and side view images of 4:8-DAC/GEL scaffold (**k**), Tubular construct printed with 4:8-DAC/GEL (**l**).

pressure and nozzle speed. Figure 5f shows the designed scaffold consisting of four layers in total and perpendicular filaments in adjacent layers. As shown in Fig. 5g–i, scaffolds were printed in different shapes (circle, regular hexagon, square) under the optimized conditions (0.15 MPa, 30 mm s^{-1}). The magnified photograph and the oblique and side view images of the scaffold (Fig. 5 k) are shown in Fig. 5j, k, respectively. All the scaffolds exhibited good architecture and fidelity. There were two main reasons for the good printability. One reason was that the optimized printing parameters were appropriate for the hydrogel. The other reason was the characteristics of the bio-ink itself, including a suitable viscosity for the successful flow through the needle of the printer, and a high storage modulus (G'), which contributed to a good shape fidelity for the scaffolds. Kim et al. fabricated a construct using COL bio-ink. In their work, pores in the scaffold started to collapse and could not distribute evenly when the height of scaffold was higher than 4 mm [9]. That was due to the poor mechanical property of COL used as only printing material. In our work, a tubular construct was also fabricated. We observed from Fig. 5i that the tubular construct could still maintain a good structure and remain upright up to 2 cm in height. This phenomenon further presented a good mechanical strength of the 4:8-DAC/GEL bio-ink.

Crosslinking efficiency

According to the 3D printing results, the 4:8-DAC/GEL hydrogel incubated for 3 h showed good printability, and the printed scaffolds exhibited good shape fidelity. However, the crosslinking reaction between the DAC and GEL continued in the freshly printed scaffolds. Therefore, it was necessary for us to further investigate the crosslinking efficiency and optimize the crosslinking conditions for freshly printed scaffolds.

As shown in Table 3, the crosslinking efficiency for the freshly printed scaffold, which had been incubated for 3 h at 37 °C before being printed, was only 40.23%. When we kept the crosslinking time constant at 21 h but increased the crosslinking temperature, the crosslinking efficiencies were 48.31, 54.34, 61.57 and 70.48% for the scaffolds crosslinked at 0, 7, 17, and 27 °C, respectively. These results indicated that the crosslinking efficiency increased with increasing temperature. This occurred because higher temperatures increase the activity of molecules, which is beneficial for accelerating the reaction. Moreover, at 37 °C, the maximum number of aldehyde groups is available for crosslinking with the amino groups of GEL; thus, crosslinking efficiency remained constant above this temperature. In addition, we kept the temperature constant at 37 °C but varied the crosslinking time from 0 to 29 h. The crosslinking efficiency increased with increasing crosslinking time and reached a constant value of 80.16% at 21 h. Therefore, the just printed scaffold could be kept for 21 h at 37 °C for a complete crosslinking reaction.

Kanth et al. [43] stabilized type I COL using DAC. In their work, the COL was treated with a 1% DAC suspension, and the resulting crosslinking efficiency reached a maximum of 94.16% after treatment at 25 °C for 24 h. Pietrucha et al. mixed a COL solution (0.5%, w/v) with a DAC suspension (1%, w/v) at a ratio of 1:1 and allowed the crosslinking reaction to continue for 24 h at 25 °C. The resulting crosslinking efficiency was 51% [44]. Our result of 80.16% was notably different from the reports by S. Kanth and K. Pietrucha, this was probably because the different mass ratio of reactants.

Physical characteristics of crosslinked scaffold

A macro-photograph of the crosslinked scaffold is shown in Fig. 6a. It is observed that the printed scaffold after crosslinking could maintain good structures and pore shapes. The crosslinked scaffold after lyophilization also had good structural integrity as shown in Fig. 6b, c. Many micropores observed on the filaments, as shown in Fig. 6d, were caused by the volatilization of aqueous water.

The size of the crosslinked scaffold shrunk compared to that of the fresh scaffold, and the shrinkage

Table 3 Crosslinking efficiency of 4:8-DAC/GEL scaffolds at different temperatures and times

Crosslinking time (h)	Temperature (°C)	Crosslinking efficiency (%)	Crosslinking time (h)	Temperature (°C)	Crosslinking efficiency (%)
21	0	48.31 ± 0.19[a]	0	37	40.23 ± 0.14[f]
21	7	54.34 ± 0.25[b]	5	37	56.72 ± 0.32[g]
21	17	61.57 ± 0.39[c]	13	37	67.72 ± 0.41[h]
21	27	70.48 ± 0.47[d]	21	37	80.16 ± 0.56[i]
21	47	80.54 ± 0.61[e]	29	37	80.83 ± 0.67[j]

Crosslinking efficiency values represent the mean ± SD of three replicates.

Crosslinking efficiency values with different superscripts are significantly different ($P < 0.05$).

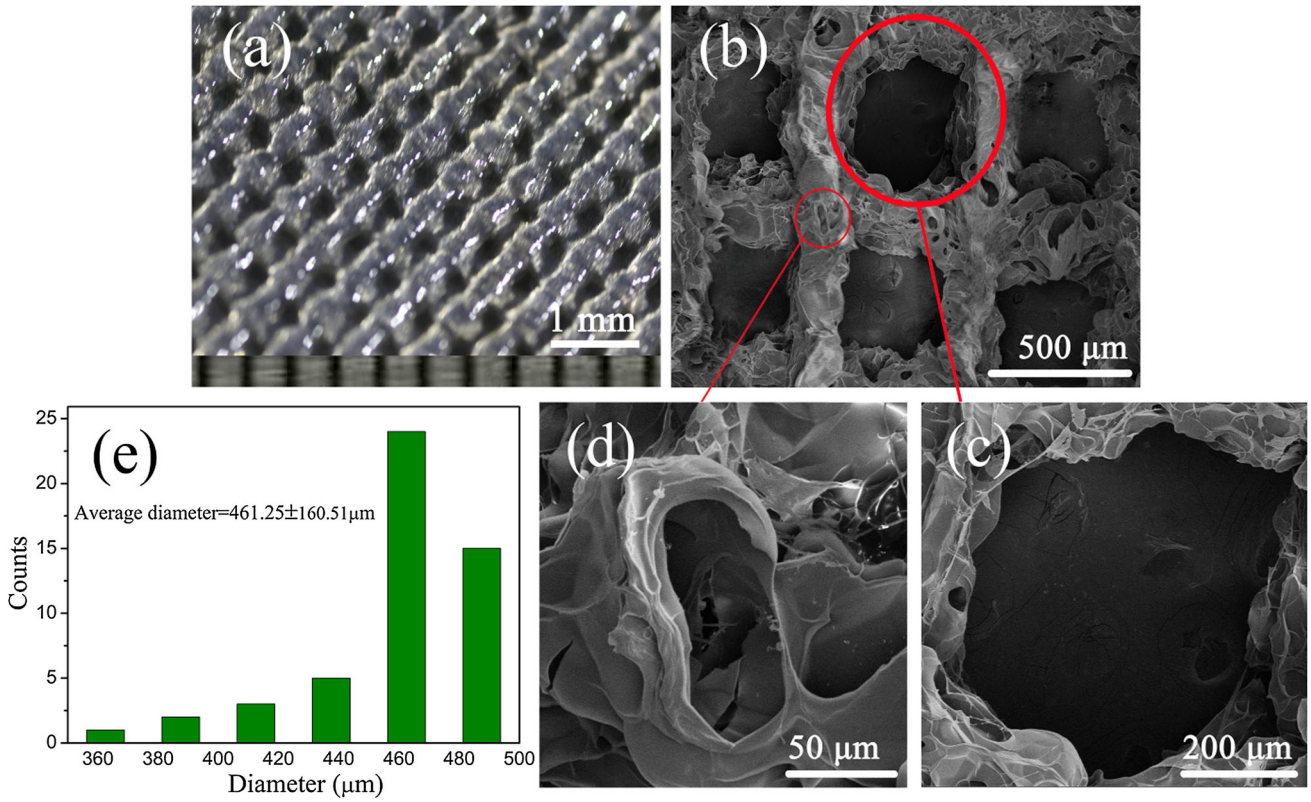

Figure 6 Morphology of the printed 4:8-DAC/GEL scaffold after crosslinking at 37 °C for 21 h (**a**). SEM images (**b**), (**c**), (**d**) of the printed 4:8-DAC/GEL scaffold after crosslinking at 37 °C for 21 h followed by lyophilization. Pore size distribution (**e**).

Table 4 Physical properties of the 4:8-DAC/GEL scaffold

Sample	Shrinkage rate (%)	Porosity (%)	Water absorption (%)
4:8-DAC/GEL scaffold	6.04 ± 0.21	95.14 ± 2.43	4756 ± 79.12

Crosslinking efficiency values represent the mean ± SD of three replicates

rate was up to 6.04% (Table 4). The crosslinking reaction between GEL and DAC molecules could form more compact structure resulting in a size shrinkage for the crosslinked scaffold. Similar phenomenon has been reported by Zhang et al. [45].

Many researchers have shown that printing a 3D porous network plays an important role in cell

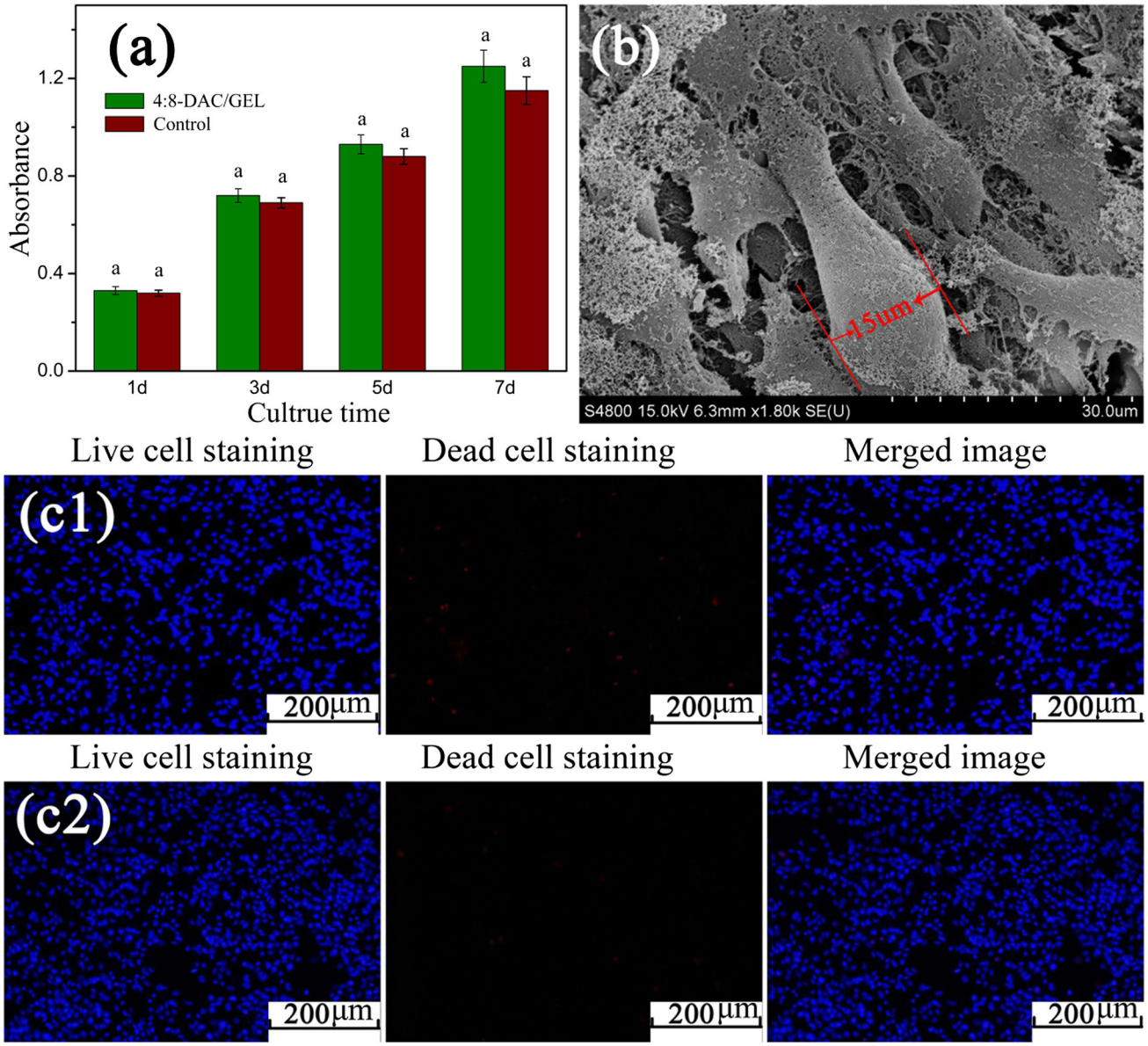

Figure 7 CCK-8 cytotoxicity test results (**a**). The same letters indicate no significant difference between 4:8-DAC/GEL and the control ($P > 0.05$). SEM image of 3T3 cells cultured in the 4:8-DAC/GEL hydrogel for 7 days (**b**). Images of live/dead cell staining after culturing cells in leaching liquor of the 4:8-DAC/GEL hydrogel for 4 days (c1); the control test (c2).

viability and ECM deposition [28]. The pore size distribution is shown in Fig. 6f. The pore diameter was mainly distributed in the range from 450 to 500 μm. The average diameter of the crosslinked scaffold was 461.25 μm. Compared with the designed scaffold (with a pore diameter of 500 μm), the crosslinked scaffold had smaller pore diameter. It was a coefficient consequence of the shrinkage and a small collapse, which occurred in the process of 3D printing due to the gravity action.

Scaffolds applied in the human body need to not only provide a 3D space and a good growth environment but also absorb nutrients to support cell proliferation. Thus, porosity and water absorption are important indices. Lu et al. [28] prepared a dialdehyde cellulose nanofiber crosslinked collagen (NCF/COL) aerogel through traditional lyophilization, and the resulting porosity and water absorption values were 90.48 and 4478%, respectively. In our work, the porosity and water absorption values for

the crosslinked scaffold after lyophilization were improved to 95.14 and 4856%, respectively. These results confirmed the superiority of 3D printing, which offers control over fine structural aspects of a scaffold, especially the pore size, resulting in the controllable adjustment of both porosity and water absorption.

Cell viability and proliferation

The cell growth inhibition of the 4:8-DAC/GEL hydrogel as a scaffold material for TE was assessed by CCK-8 assay. The leaching liquor of the 4:8-DAC/GEL hydrogel was used to culture cells in this study. As shown in Fig. 7a, the optical density (OD) showed a gradual increase with increasing culture time, and there was no significant difference in the OD between the 4:8-DAC/GEL and the control. This result indicated that the leaching liquor of the DAC/GEL hydrogel could support cell growth and proliferation.

To observe differences in the morphology of the 3T3 cells, 3T3 cells were seeded in the 4:8-DAC/GEL hydrogel and cultured for 7 days. Figure 7b shows that multiple layers of 3T3 cells in the hydrogel coating; cells exhibited a spindle shape with a diameter of approximately 15 μm and pseudopod extension, which indicated that these cells grew well. These results confirmed that the DAC/GEL hydrogel could support the growth of 3T3 cells and provide channels for the migration and proliferation of 3T3 cells.

Apoptosis induced by the DAC/GEL hydrogel was evaluated using the leaching liquor of the 4:8-DAC/GEL hydrogel. Live/dead staining was performed to inspect cell viability visually after 48 h. As shown in Fig. 7c, viable fibroblasts are shown in blue, while dead cells are shown in red. More viable than dead 3T3 cells were observed. Moreover, there were minor differences in the number of dead cells between the DAC/GEL sample and the control. These results indicated that the DAC/GEL hydrogel did not obviously induce apoptosis above the background level.

Conclusions

In summary, this study reported a new bio-ink composed of and GEL and DAC which played a role as a natural crosslinker. The optimal 4:8-DAC/GEL hydrogel exhibited a low swelling ratio and a high mechanical strength nearly 41.3-fold greater than that of the GEL hydrogel. Rheological tests further confirmed that the 4:8-DAC/GEL incubated for 3 h had a high storage modulus (G') and a viscosity suitable for 3D printing. Then, 4:8-DAC/GEL scaffolds were successfully printed by optimizing the printing pressure and nozzle speed. Subsequently, the freshly printed scaffold was subjected to an additional crosslinking reaction under optimized conditions, resulting in a crosslinked scaffold with good shape fidelity and reproducibility. The biocompatibility tests suggested that the 4:8-DAC/GEL hydrogel exerted no obvious cytotoxicity. These characteristics confirmed that the 4:8-DAC/GEL hydrogel has potential as bio-ink for 3D printing.

Acknowledgements

This research was supported by the Excellent Doctoral Thesis Support Program of Yangzhou University, the City and School Cooperation Project, the Top Talents Support Program of Yangzhou University, the Natural Science Foundation of China (81770018).

Electronic supplementary material: The online version of this article (https://doi.org/10.1007/s10853-018-2407-0) contains supplementary material, which is available to authorized users.

References

[1] Zhang YS, Yue K, Aleman J et al (2017) 3D bioprinting for tissue and organ fabrication. Ann Biomed Eng 45(1):148–163

[2] Zhang X, Yang Y, Yao J, Shao Z, Chen X (2014) Strong collagen hydrogels by oxidized dextran modification. ACS SustaiChem Eng 2(5):1318–1324

[3] Li H, Liu S, Lin L (2016) Rheological study on 3D printability of alginate hydrogel and effect of graphene oxide. Int J Bioprinting 2(2):54–66

[4] Abbadessa A, Blokzijl MM, Mouser VH et al (2016) A thermo-responsive and photo-polymerizable chondroitin sulfate-based hydrogel for 3d printing applications. Carbohydr Polym 149:163–174

[5] Christensen K, Xu C, Chai W, Zhang Z, Fu J, Huang Y (2015) Freeform inkjet printing of cellular structures with bifurcations. Biotechnol Bioeng 112(5):1047–1055

[6] Duan B, Hockaday LA, Kang KH et al (2013) 3D bioprinting of heterogeneous aortic valve conduits with alginate/gelatin hydrogels. J Biomed Mater Res Part A 101A(5):1255–1264

[7] Colosi C, Shin SR, Manoharan V et al (2016) Microfluidic bioprinting of heterogeneous 3d tissue constructs using low viscosity bioink. Adv Mater 28(4):677–681

[8] Lee VK, Kim DY, Ngo H et al (2014) Creating perfused functional vascular channels using 3d bio-printing technology. Biomaterials 35(28):8092–8102

[9] Kim Y, Lee H, Kim G (2016) Strategy to achieve highly porous/biocompatible macroscale cell blocks, using a collagen/genipin-bioink and an optimal 3D printing process. ACS Appl Mater Interfaces 8(47):32230–32240

[10] Aleksander S, David M, Edi K et al (2012) Bioprinted amniotic fluid-derived stem cells accelerate healing of large skin wounds. Stem Cells Transl Med 1(11):792–802

[11] Highley CB, Rodell CB, Burdick JA (2015) Direct 3d printing of shear-thinning hydrogels into self-healing hydrogels. Adv Mater 27(34):5075–5079

[12] Muller WEG, Neufurth M, Tolba E et al (2015) A new printable and durable n, o-carboxymethyl chitosan-ca2 + -polyphosphate complex with morphogenetic activity. J Mater Chem B 3(8):1722–1730

[13] Zhang X, Yang Y, Yao J et al (2014) Strong collagen hydrogels by oxidized dextran modification. Acs Sustain Chem Eng 2(5):1318–1324

[14] Tan YJ, Tan X, Yeong WY et al (2016) Hybrid microscaffold-based 3D bioprinting of multi-cellular constructs with high compressive strength: a new biofabrication strategy. Sci Rep 6:39140

[15] Kim YB, Lee H, Kim GH (2016) Strategy to achieve highly porous/biocompatible macroscale cell blocks, using a collagen/genipin-bioink and an optimal 3D printing process. Acs Appl Mater Interfaces 8(47):32230–32240

[16] Kim T, Sridharan I, Zhu B, Effect of CNT on collagen fiber structure et al (2015) Stiffness assembly kinetics and stem cell differentiation. Mater Sci Eng C Mater Biol Appl 49:281–289

[17] Peppas N, Hilt J, Khademhosseini A et al (2006) Hydrogels in biology and medicine: from molecular principles to bionanotechnology. Adv Mater 18(11):1345–1360

[18] Henriksson I, Gatenholm P, Hägg DA (2017) Increased lipid accumulation and adipogenic gene expression of adipocytes in 3D bioprinted nanocellulose scaffolds. Biofabrication 9(1):015022

[19] Piras CC, Fernándezprieto S, De Borggraeve WM (2017) Nanocellulosic materials as bioinks for 3D bioprinting. Biomater Sci 5:1988–1992

[20] Murphy CA, Collins MN (2016) Microcrystalline cellulose reinforced polylactic acid biocomposite filaments for 3D printing. Polym Compos 15:236–244

[21] Nguyen D, Hägg DA, Forsman A et al (2017) Cartilage tissue engineering by the 3D bioprinting of iPS cells in a nanocellulose/alginate bioink. Sci Reports 7(1):658

[22] Markstedt K, Mantas A, Tournier I et al (2015) 3D bioprinting human chondrocytes with nanocellulose alginate bioink for cartilage tissue engineering applications. Biomacromol 16(5):1489–1496

[23] Ávila HM, Schwarz S, Rotter N et al (2016) 3D bioprinting of human chondrocyte-laden nanocellulose hydrogels for patient-specific auricular cartilage regeneration. Bioprinting 1(2):22–35

[24] Müller M, Öztürk E, Arlov O et al (2016) Alginate sulfate-nanocellulose bioinks for cartilage bioprinting applications. Ann Biomed Eng 45(1):210–223

[25] Sawkins MJ, Mistry P, Brown BN et al (2015) Cell and protein compatible 3D bioprinting of mechanically strong constructs for bone repair. Biofabrication 7(3):035004

[26] Torres-Rendon JG, Koepf M, Gehlen D et al (2016) Cellulose nanofibril hydrogel tubes as sacrificial templates for freestanding tubular cell constructs. Biomacromol 17:905–913

[27] Siqueira G, Kokkinis D, Libanori R et al (2017) Cellulose nanocrystal inks for 3D printing of textured cellular architectures. Adv Funct Mater 27(12):1604619

[28] Lu T, Li Q, Chen W, Yu H (2014) Composite aerogels based on dialdehyde nanocellulose and collagen for potential applications as wound dressing and tissue engineering scaffold. Compos Sci Technol 94(4):132–138

[29] Jiang Y, Zhou J, Zhang Q et al (2017) Preparation of cellulose nanocrystals from humulus japonicus stem and the influence of high temperature pretreatment. Carbohydr Polym 64:284–293

[30] Iii CMO, Bubnis WA (1996) Chemical and swelling evaluations of amino group crosslinking in gelatin and modified gelatin matrices. Pharm Res 13(12):1821–1827

[31] Zhang R, Ma PX (1999) Poly(alpha-hydroxyl acids)/hydroxyapatite porous composites for bone-tissue engineering I preparation and morphology. J Biomed Mater Res 44(4):446–455

[32] Chen W, Yu H, Li Q, Liu Y, Li J (2011) Ultralight and highly flexible aerogels with long cellulose nanofibers. Soft Matter 7(21):10360–10368

[33] Sain M, Panthapulakkal S (2006) Bioprocess preparation of wheat straw fibers and their characterization. Ind Crops Prod 23(1):1–8

[34] Alemdar A, Sain M (2008) Isolation and characterization of nanofibers from agricultural residues-wheat straw and soy hulls. Biores Technol 99(6):1664–1671

[35] Münster L, Vícha J, Klofáč J, Masař M, Kucharczyk P, Kuřitka I (2017) Stability and aging of solubilized dialdehyde cellulose. Cellulose 24(7):1–14

[36] Pietrucha K, Safandowska M (2015) Dialdehyde cellulose-crosslinked collagen and its physicochemical properties. Process Biochem 50(12):2105–2111

[37] Dorris GM, Gray DG (1978) Surface analysis of paper and wood fibres by ESCA II surface composition of mechanical pulps. Cellul Chem Technol 12:721–734

[38] Gao C, Yan T, Dai K, Wan Y (2012) Immobilization of gelatin onto natural nanofibers for tissue engineering scaffold applications without utilization of any crosslinking agent. Cellulose 19(3):761–768

[39] Hayami JWS, Waldman SD, Amsden BG (2015) Photo-cross-linked methacrylated polysaccharide solution blends with high chondrocyte viability, minimal swelling, and moduli similar to load bearing soft tissues. Eur Polym J 72:687–697

[40] Das S, Pati F, Choi YJ et al (2015) Bioprintable, cell-laden silk fibroin-gelatin hydrogel supporting multilineage dif‘ ferentiation of stem cells for fabrication of three-dimensional tissue constructs. Acta Biomater 11(1):233–246

[41] Wei LN, Yeong WY, Naing MW (2016) Polyelectrolyte gelatin-chitosan hydrogel optimized for 3d bioprinting in skin tissue engineering. Int J Bioprinting 2(1):53–62

[42] Yashima S, Takase N, Kurokawa T, Gong JP (2014) Friction of hydrogels with controlled surface roughness on solid flat substrates. Soft Matter 10(18):3192–3199

[43] Kanth SV, Ramaraj A, Rao JR, Nair BU (2015) Stabilization of type I collagen using dialdehyde cellulose. Process Biochem 4:869–874

[44] Huang S, Yao B, Xie J, Fu X (2016) 3d bioprinted extracellular matrix mimics facilitate directed differentiation of epithelial progenitors for sweat gland regeneration. Acta Biomater 32:170–177

[45] Zhang S, Huang Y, Yang X et al (2009) Gelatin nanofibrous membrane fabricated by electrospinning of aqueous gelatin solution for guided tissue regeneration. J Biomed Mater Res Part A 90(3):671–679